Spectrochimica Acta Part A 76 (2010) 161–173

Contents lists available at ScienceDirect

Spectrochimica Acta Part A: Molecular and Biomolecular Spectroscopy

journal homepage: www.elsevier.com/locate/saa

Spectral, magnetic, biocidal screening, DNA binding and photocleavage studies of mononuclear Cu(II) and Zn(II) metal complexes of tricoordinate heterocyclic Schiff base ligands of pyrazolone and semicarbazide/thiosemicarbazide based derivatives

N. Raman [a,*], A. Selvan [a], P. Manisankar [b]

[a] Research Department of Chemistry, VHNSN College, Virudhunagar, Tamil Nadu 626001, India
[b] Department of Industrial Chemistry, Alagappa University, Karaikudi 630003, India

ARTICLE INFO

Article history:
Received 7 January 2010
Received in revised form 24 February 2010
Accepted 11 March 2010

Keywords:
Schiff base
Metal complexes
DNA interaction
Photocleavage
Tricoordinate ligand
Antimicrobial study

ABSTRACT

We depict the synthesis and characterization of copper(II) and zinc(II) coordination compounds of 4-(3′,4′-dimethoxybenzaldehydene)2-3-dimethyl-1-phenyl-3-pyrazolin-5-semicarbazone (**1a**), 4-(3′,4′-dimethoxybenzaldehydene)2-3-dimethyl-1-phenyl-3-pyrazolin-5-thiosemicarbazone (**1b**), 4-(3′-hydroxy-4′-nitrobenzaldehydene)2-3-dimeth yl-1-phenyl-3-pyrazolin-5-semicarbazone (**1c**) and 4-(3′-hydroxy-4′-nitrobenzal dehydene)2-3-dimethyl-1-phenyl-3-pyrazolin-5-thiosemicarbazone (**1d**). All the remote compounds have the general composition $[ML_2]$ (M = Cu(II) and Zn(II)); L = Schiff base (**1a**–**1d**). All the complexes were characterized by elemental analysis, molar conductivity, IR, ^{1}H NMR, UV–vis, ESI-Mass, magnetic susceptibility measurements, cyclic voltammetric measurements, and EPR spectral studies. It has been originated that the Schiff bases with Cu(II) and Zn(II) ions form mononuclear complexes on 1:2 (metal:ligand) stoichiometry. Distorted octahedral environment is suggested for the metal complexes. The conductivity data confirm the non-electrolytic nature of the complexes. The interaction of CuL_2 **[1a–1d]** complexes with CT DNA was investigated by spectroscopic, electrochemical and viscosity measurements. Results suggest that the copper complexes bind to DNA *via* an intercalative mode. Moreover, the complexes have been found to promote the photocleavage of plasmid DNA pBR322 under irradiation at 365 nm. The Schiff bases and their metal complexes were screened for their antifungal and antibacterial activities against different species of pathogenic fungi and bacteria and their biopotency has been discussed.

1. Introduction

Schiff bases are important class of ligands in coordination chemistry and found extensive application in different fields of science. Schiff bases of semicarbazones/thiosemicarbazones have aroused with significant interest in the field of chemistry and biology due to their antibacterial, antifungal, antimalarial, antineoplastic and antiviral activities [1]. The biological activities of semicarbazones/thiosemicarbazones are considered to be related to their ability to form chelates with metals. The chemistry of transition metal complexes of semicarbazones/thiosemicarbazones based Schiff bases has been receiving significant attention because of their pharmacological properties. The biological activities of metal complexes differ from those of either the free ligands or metal ions and increased or decreased activities in relation to the non-complexed semicarbazones/thiosemicarbazones have been reported for several transition metal complexes [2]. Among the metal complexes of semicarbazones/thiosemicarbazones, the Cu(II) and Zn(II) chelates have been especially studied regarding their antitumour potentials [3]. Moreover, Cu(II) and Zn(II) complexes with oxygen, sulphur and nitrogen containing ligands are the subject of intensive biological evaluation in the search for less toxic and more selective anticancer therapies [4,5]. Especially heterocyclic thiosemicarbazones have been the subject of extensive investigation because of their wide use in biological field [6–8].

The investigation of metal complexes with Schiff bases derived from pyrazole, *e.g.*, 4-amino-2-3-dimethyl-1-phenyl-3-pyrazolin-5-one, is interesting because of the fact that these compounds can serve as models for studying a wide range of biological reactions which are catalyzed by enzymes. It has been shown that in the presence of metal ions, free pyrazole can catalyze many reactions like carbonylation, hydroformylation, oxidation, reduction and epoxidation [9]

* Corresponding author.
E-mail address: drn_raman@yahoo.co.in (N. Raman).

1386-1425/$ – see front matter © 2010 Elsevier B.V. All rights reserved.
doi:10.1016/j.saa.2010.03.007

Considering the significance of semicarbazones/thiosemicarbazones and pyrazolone derivatives, we have synthesized the Schiff bases (**1a**–**1d**) and their Cu(II) and Zn(II) complexes. It is well known that a general study on structure and bonding can help in better understanding of the complex life processes. Hence, the structures of the synthesized Schiff bases and their complexes were elucidated by analytical and spectral studies. Their biological studies like antimicrobial and DNA binding and cleavage were carried out in order to understand the mode of interaction of the synthesized Schiff bases and their complexes with Calf thymus DNA (CT DNA).

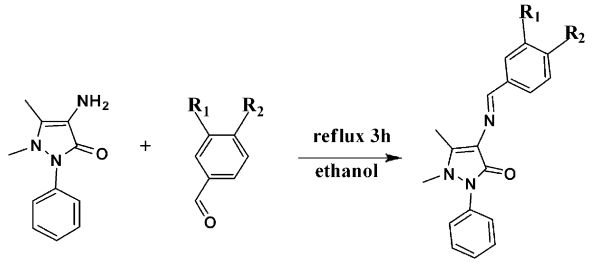

Scheme 1. Preparation of 4-(3′,4′-benzaldehydene)2-3-dimethyl-1-phenyl-3-pyrazolin-5-one.

2. Experimental

2.1. Chemicals

All reagents and solvents were of AR grade, purchased commercially. Tris–HCl buffer salts were purchased from Qualigens (India); CT DNA and pBR322 DNA from Bangalore Genei, India. Tris–HCl buffer solution [5 mM Tris–HCl and 50 mM NaCl (pH 7.2); Tris = Tris(hydroxymethyl) aminomethane] was prepared using deionised double distilled water.

All DNA stock solutions (1000 mg/L) were prepared with the Tris–HCl buffer solution and kept frozen. More dilute solutions were prepared with 50 mM Tris–HCl (pH 7.2). The concentration of CT DNA was measured by using its known extinction coefficient at 260 nm (6600 M^{-1} cm^{-1}) [10]. The absorbance at 260 nm (A_{260}) and at 280 nm (A_{280}) for CT DNA was measured to ensure its purity. The ratio A_{260}/A_{280} was found to be 1.84, indicating that CT DNA was satisfactorily free from protein.

2.2. Physical measurements

UV–vis spectra were recorded on a Shimadzu Model 1601 UV-Visible Spectrophotometer. IR spectra were recorded (KBr) with a PerkinElmer FTIR-1605 spectrophotometer. ^{1}H NMR spectra were taken on a Varian XL-300 MHz spectrometer with tetramethylsilane (TMS) as the internal standard at room temperature. The complexes were analyzed for their metal contents, following standard procedures [11] after decomposition with a mixture of conc. HNO_3 and HCl, followed by conc. H_2SO_4. Microanalyses were carried out on a PerkinElmer 240 elemental analyzer. Mass spectrometry experiments were performed on a JEOL-AccuTOF JMS-T100LC mass spectrometer equipped with a custom-made electrospray interface (ESI). The X-band EPR spectra of the complexes were recorded at RT (300 K) and LNT (77 K) using TCNE as the *g*-marker. Room temperature magnetic susceptibility measurements were carried out on a modified Gouy-type magnetic balance, Hertz SG8-5HJ. The molar conductivity of the complexes in DMF solution (10^{-3} M) was measured using a conductometer model 601/602.

Voltammetric experiments were performed on a CHI 620C electrochemical analyzer in freshly distilled DMF solutions. 0.1 M tetrabutylammonium perchlorate (TBAP) was used as the supporting electrolyte. The three-electrode cell comprised a reference Ag/AgCl, auxiliary Pt and the working glassy carbon electrodes. All the solutions examined by electrochemical techniques were purged with nitrogen for 10 min prior to each set of experiments. All measurements were carried out at room temperature (25 °C).

2.3. Biocidal screening

Antibacterial and antifungal activities of the antibiotics and the metal complexes were screened against four pathogenic bacteria, *viz. Staphylococcus aureus*, *Bacillus subtilis*, *Escherichia coli*, and *Pseudomonas putita* and four fungi, *viz. Aspergillus niger*, *Rhizopus stolonifer*, *Candida albicans* and *Rhizoctonia bataicola*. For the detection of the biocidal activities, the filter paper disc agar diffusion method was used [12–14]. The minimum inhibitory concentration (MIC) was considered to be the lowest concentration, which exhibited the same turbidity as the blank tube. Pure Streptomycin and Nystatin were used separately as standards for antibacterial and antifungal activity tests respectively. Nutrient agar (NA) was used as basal medium for the cultured bacteria. A series of different concentrations of the compounds in dimethylformamide (DMF) solvent were placed on the surface of the culture and incubated at 37 °C for 24 h for the bacterial culture. The antifungal activities were performed with potato agar medium in DMF as solvent and incubated at 37 °C for 48–72 h.

2.4. Synthesis

2.4.1. Preparation of 4-(3′, 4′-benzaldehydene)2-3-dimethyl-1-phenyl-3-pyrazolin-5-one

The reaction of 4-amino-2-3-dimethyl-1-phenyl-3-pyrazolin-5-one with 3,4-dimethoxybenzaldehyde and 3-hydroxy-4-nitrobenzaldehyde, carried out for the preparation of 4-(3′,4′-benzaldehydene)2-3-dimethyl-1-phenyl-3-pyrazolin-5-one is shown in Scheme 1.

The Schiff bases under investigation were prepared by mixing an ethanol solution (25 mL) of 4-amino-2-3-dimethyl-1-phenyl-3-pyrazolin-5-one (2.032 g, 0.01 mol) with 3,4-dimethoxybenzaldehyde (1.66 g, 0.01 mol) and 3-hydroxy-4-nitrobenzaldehyde (1.67 g, 0.01 mol) in the same volume of ethanol and refluxing for 3 h in water bath, the precipitate formed was collected and recrystallized from ethanol.

4-(3′,4′-Dimethoxybenzaldehydene)2-3-dimethyl-1-phenyl-3-pyrazolin-5-one is light yellow crystal and its yield is 89%. Anal. calcd. $C_{20}H_{21}N_3O_3$ M.W.: 351.40, C(68.36%), H(6.02%), N(11.95%), found: C(68.25%), H(5.92%), N(11.48%); ^{1}H NMR (DMSO-d6) δ: 3.28(s, 3H, P_Z–N–CH_3), 2.26(s, 3H, P_Z–C–CH_3), 3.92(s, 3H, O–CH_3), 6.97–7.40(m, 3H, Ph), 6.90–7.37(m, 5H, Ph), 8.01(s, 1H, N=CH); IR (KBr) ν (cm^{-1}): 1634(strong, s) (HC=N), 1308(s) (O–CH_3), 1281(s) (P_Z–C–CH_3), 1181(s) (P_Z–N–CH_3), 1714(s) (P_Z–C=O), 1471(s) (Ph–C=C), 1545(medium, m) (Ph–C–C), 3048(s) (Ph–C–H).

4-(3′-Hydroxy-4′-nitrobenzaldehydene)2-3-dimethyl-1-phenyl-3-pyrazolin-5-one is yellow powder and its yield is 85%. Anal. calcd. $C_{18}H_{16}N_4O_4$ M.W.: 352.35, C(61.35%), H(4.57%), N(15.90%), found: C(68.25%), H(4.43%), N(15.48%); ^{1}H NMR (DMSO-d6) δ: 3.11(s, 3H, P_Z–N–CH_3), 2.58(s, 3H, P_Z C–CH_3), 10.28(s, 1H, OH), 6.77–7.15(m, 3H, Ph), 6.90–7.37(m, 5H, Ph), 8.00(s, 1H, N=CH); IR (KBr) ν (cm^{-1}): 1614(s) (HC=N), 1608(weak, w) (C–NO_2), 3442(broad, b) (OH), 1293(s) (P_Z–C–CH_3), 1145(s) (P_Z–N–CH_3), 1651(s) (P_Z–C=O), 1423(s) (Ph–C=C), 1530(m) (Ph–C–C), 3075(s) (Ph–C–H).

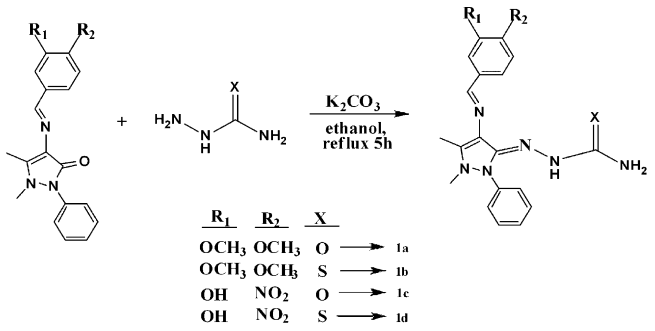

Scheme 2. Preparation of 4-(3′,4′-benzaldehydene)2-3-dimethyl-1-phenyl-3-pyrazolin-5-semicarbazone/thiosemicarbazone.

2.4.2. Preparation of 4-(3′,4′-benzaldehydene)2-3-dimethyl-1-phenyl-3-pyrazolin-5-semicarbazone/thiosemicarbazone

The reaction of 4-(3′,4′-benzaldehydene)2-3-dimethyl-1-phenyl-3-pyrazolin-5-one with semicarbazide (l.11 g, 0.01 mol)/thiosemicarbazide (0.91 g, 0.01 mol) in ethanol was refluxed for 4–5 h to produce Schiff bases (**1a**–**1d**). This is shown in Scheme 2. After cooling to room temperature, light yellow product obtained was filtered and washed with ethanol.

1a is light yellow powder and its yield is 75%. Anal. calcd. $C_{21}H_{24}N_6O_3$ M.W.: 408.45, C(61.75%), H(5.92%), N(20.57%), found: C(61.20%), H(6.04%), N(19.65%); ^{1}H NMR (DMSO-d6) δ: 2.21(s, 3H, P_Z–C–CH_3), 2.87(s, 3H, P_Z–N–CH_3), 6.85(s, 2H, NH_2), 3.71(s, 3H, O–CH_3), 6.91–7.36(m, 5H, Ph), 7.59–7.68(m, 3H, Ph), 8.28(s, 1H, N=CH), 9.66(s, 1H, NH-sc); IR (KBr) ν (cm^{-1}): 3180–3224(b) (NH_2), 3069(b) (–NH–Sc),1698(s) (Sc–C=O), 1589(s) (C=N), 1324(m) (O–CH_3), 1266(s) (P_Z–C–CH_3), 1167(s) (P_Z–N–CH_3), 1422(m) (Ph–C=C), 1518(s) (Ph–C–C), 2932(s) (Ph–C–H).

1b is also light yellow powder and its yield is 80%. Anal. calcd. $C_{21}H_{24}N_6O_2S$ M.W.: 424.52, C(59.41%), H(5.69%), N(19.79%), S(7.55%), found: C(59.20%), H(6.04%), N(19.65%), S(7.45%); ^{1}H NMR (DMSO-d6) δ: 2.15(s, 3H, P_Z C–CH_3), 2.85(s, 3H, P_Z–N–CH_3), 6.39(s, 2H, NH_2), 3.92(s, 3H, O–CH_3), 7.08–7.48(m, 5H, Ph), 7.56–7.81(m, 3H, Ph), 8.41(s, 1H, N=CH), 9.69(s, 1H, NH-tsc); IR (KBr) ν (cm^{-1}): 3188–3273(b) (NH_2), 3163(b) (–NH-tsc), 834(m) (C=S), 1626(m) (C=N), 1335(s) (O–CH_3), 1262(m) (P_Z–C–CH_3), 1133(b) (P_Z–N–CH_3), 1420(s) (Ph–C=C), 1534(m) (Ph–C–C), 2929(b) (Ph–C–H).

1c is light yellow powder and its yield is 65%. Anal. calcd. $C_{19}H_{19}N_7O_4$ M.W.: 409.40, C(55.74%), H(4.67%), N(23.94%), found: C(54.85%), H(4.27%), N(23.45%); ^{1}H NMR (DMSO-d6) δ: 2.24(s, 3H, P_Z C–CH_3), 2.93(s, 3H, P_Z–N–CH_3), 6.43(s, 2H, NH_2), 10.56(s, 1H, OH), 6.91–7.26(m, 5H, Ph), 7.44–7.60(m, 3H, Ph), 8.45 (s,1H, N=CH), 9.88(s, 1H, NH-Sc); IR (KBr) ν (cm^{-1}): 3268(s) (NH_2), 3127(b) (–NH–Sc), 1618(m) (C=N), 1603(w) (C–NO_2), 3357(s) (OH), 1270(s) (P_Z–C–CH_3), 1147(s) (P_Z–N–CH_3), 1651(w) (Sc–C=O), 1418(m)(Ph–C=C), 1511(s) (Ph–C–C), 2966(b) (Ph–C–H)

1d is also a light yellow powder and its yield is 65%. Anal. calcd. $C_{19}H_{19}N_7O_3S$ M.W.: 425.46, C(53.63%), H(4.50%), N(23.04%), S(7.53%), found: C(54.85%), H(4.27%), N(23.45%), S(7.32%); ^{1}H NMR (DMSO-d6) δ: 2.51(s, 3H, P_Z C–CH_3), 3.02–3.41(s, 3H, P_Z–N–CH_3), 6.38(s, 2H, NH_2),10.75(s, 1H, OH), 7.35–7.58(m, 5H,Ph), 7.85–7.98(m, 3H, Ph), 8.18(s, 1H, N=CH), 9.57(S, 1H, NH-tsc); IR (KBr) ν (cm^{-1}): 3279(s) (NH_2), 3126(b) (–NH-tsc), 1615(m) (C=N), 1606(w) (C–NO_2), 3469(s) (OH), 1265(m) (P_Z–C–CH_3), 1195(s) (P_Z–N–CH_3), 828(m) (C=S), 1455(m) (Ph–C=C), 1545(s) (Ph–C–C), 2948(s) (Ph–C–H).

2.4.3. Synthesis and characterization of the complexes

*2.4.3.1. Cu(II) complexes of **1a**–**1d**.* All the complexes were prepared by mixing ethanolic solution of ligands and metal salts in required molar ratio (2:1). The reaction mixture was refluxed on a water bath for 2–3 h and then concentrated to a small volume on a hot plate at ~50 °C. After cooling, the complexes obtained were filtered, recrystallized from ethanol and dried in vacuum over $CaCl_2$.

CuL_2**[1a]** is light green powder and its yield is 65%. Anal. calcd. $CuC_{42}H_{46}N_{12}O_6$ M.W.: 878.45, C(57.42%), H(5.27%), N(19.13%), Cu(7.23%) found: C(57.03%), H(4.95%), N(18.91%), Cu(6.85%); IR (KBr) ν (cm^{-1}): 3182–3219(b) (NH_2), 1060(m) (C–O), 1564(s) (C=N), 1326(m) (O–CH_3), 1262(s) (P_Z–C–CH_3), 1164(s) (P_Z–N–CH_3), 1421(m) (Ph–C=C), 1521(s) (Ph–C–C), 2930(s) (Ph–C–H), 456(s) (Cu–N), 557(m) (Cu–O).

CuL_2**[1b]** is yellow powder and its yield is 75%. Anal. calcd. $CuC_{42}H_{46}N_{12}O_4S_2$ M.W.: 910.57, C(55.40%), H(5.09%), N(18.45%), S(7.04%), Cu(6.97%) found: C(55.13%), H(4.85%), N(18.15%), S(6.85%), Cu(6.75%); IR (KBr) ν (cm^{-1}): 3186–3275(b) (NH_2), 694(s) (C–S), 1598(m) (C=N), 1332(s) (O–CH_3), 1261(m) (P_Z–C–CH_3), 1129(b) (P_Z–N–CH_3), 1421(s) (Ph–C=C), 1531(m) (Ph–C–C), 2924(b) (Ph–C–H), 458(s) (Cu–N), 364(m) (Cu–S).

CuL_2**[1c]** is light yellow powder and its yield is 60%. Anal. calcd. $CuC_{38}H_{36}N_{14}O_8$ M.W.: 880.33, C(51.84%), H(4.12%), N(22.27%), Cu(7.21%), found: C(51.20%), H(3.95%), N(21.85%), Cu(6.95%); IR (KBr) ν (cm^{-1}): 3262(s) (NH_2), 1075(m) (C–O), 1595(m) (C=N), 1602(w) (C–NO_2), 3354(s) (OH), 1273(s) (P_Z–C–CH_3), 1146(s) (P_Z–N–CH_3), 1416(m) (Ph–C=C), 1509(s) (Ph–C–C), 2963(b) (Ph–C–H), 456(s) (Cu–N), 552(m) (Cu–O).

CuL_2**[1d]** is light greenish yellow powder and its yield is 55%. Anal. calcd. $CuC_{38}H_{36}N_{14}O_6S_2$ M.W.: 912.46, C(50.02%), H(3.97%), N(21.49%), S(7.02%), Cu(6.96%) found: C(49.75%), H(3.65%), N(20.95%), S(6.95%), Cu(6.85%); IR (KBr) ν (cm^{-1}): 3279(s) (NH_2), 702(m) (C–S), 1591(m) (C=N), 1604(w) (C–NO_2), 3465(s) (OH), 1263(m) (P_Z–C–CH_3), 1192(s) (P_Z–N–CH_3), 1455(m) (Ph–C=C), 1543(s) (Ph–C–C), 2947(s) (Ph–C–H), 452(s) (Cu–N), 367(m) (Cu–S).

*2.4.3.2. Zn(II) complexes of **1a**–**1d**.* A general method was used for the preparation of the complexes. A hot ethanolic solution of the corresponding zinc(II) salt was mixed with a hot ethanolic solution of the respective ligand (in 1:2 molar ratio). The reaction mixture was refluxed on a water bath for 2–3 h. On cooling at room temperature, the desired complexes were precipitated out in each case. They were filtered, recrystallized, washed with ethanol and finally dried over $CaCl_2$ under vacuum.

ZnL_2**[1a]** is light yellow powder and its yield is 56%. Anal. calcd. $ZnC_{42}H_{46}N_{12}O_6$ M.W.: 880.28, C(57.30%), H(5.26%), N(19.09%), Zn(7.42%); found: C(56.65%), H(5.15%), N(18.87%), Zn(7.34%); ^{1}H NMR (DMSO-d6) δ: 2.28(s, 3H, P_Z–C–CH_3), 2.90(s, 3H, P_Z–N–CH_3), 6.08(s, 2H, NH_2), 3.93(s, 3H, O–CH_3), 6.90–7.26(m, 5H,Ph), 7.60–7.75(m, 3H, Ph), 8.92(s, 1H, N=CH); IR (KBr) ν (cm^{-1}): 3184–3221(b) (NH_2), 1098(m) (C–O), 1569(s) (C=N), 1323(m) (O–CH_3), 1263(s) (P_Z–C–CH_3), 1164(s) (P_Z–N–CH_3), 1421(m) (Ph–C=C), 1519(s) (Ph–C–C), 2929(s) (Ph–C–H), 459(s) (Zn–N), 553(m) (Zn-O).

ZnL_2**[1b]** is light colourless powder and its yield is 72%. Anal. calcd. $ZnC_{42}H_{46}N_{12}O_4S_2$ M.W.: 912, C(55.28%), H(5.08%), N(18.42%), S(7.02%), Zn(7.16%); found: C(55.12%), H(4.85%), N(18.28%), S(6.93%), Zn(7.07%); ^{1}H NMR (DMSO-d6) δ: 2.01(s, 3H, P_Z–C–CH_3), 3.15(s, 3H, P_Z–N–CH_3), 5.93(s, 2H, NH_2), 3.97(s, 3H, O–CH_3), 6.85–7.33(m, 5H, Ph), 7.54–7.68(m, 3H, Ph),8.87(s, 1H, N=CH); IR (KBr) ν (cm^{-1}): 3185–3274(b) (NH_2), 649(s) (C–S), 1602(m) (C=N), 1331(s) (O–CH_3), 1264(m) (P_Z–C–CH_3), 1129(m) (P_Z–N–CH_3), 1419(s) (Ph–C=C), 1531(m) (Ph–C–C), 2926(b) (Ph–C–H), 465(s) (Zn–N), 357 (s) (Zn-S).

ZnL_2**[1c]** is yellow powder and its yield is 65%. Anal. calcd. $ZnC_{38}H_{36}N_{14}O_8$ M.W.: 882.17, C(51.73%), H(4.11%), N(22.22%), Zn(7.41%); found: C(51.65%), H(4.05%), N(21.98%), Zn(7.38%); ^{1}H

NMR (DMSO-d6) δ: 2.57(s, 3H, P_Z–C–CH_3), 3.20–3.60(s, 3H, P_Z–N–CH_3), 6.34(s, 2H, NH_2), 10.59(s, 1H, OH), 7.31–7.42(m, 5H, Ph), 7.80–7.98(m, 3H, Ph), 8.58(s, 1H, N=CH); IR (KBr) ν (cm^{-1}): 3264(s) (NH_2), 1058(m) (C–O), 1591(m) (C=N), 1598(w) (C–NO_2), 3351(s) (OH), 1271(s) (P_Z–C–CH_3), 1149(s) (P_Z–N–CH_3), 1420(m) (Ph–C=C), 1507(s) (Ph–C–C), 2961(b) (Ph–C–H), 472(s) (Zn–N), 561(m) (Zn-O).

ZnL_2 **1d** is light yellow powder and its yield is 53%. Anal. calcd. Zn $C_{38}H_{36}N_{14}O_6S_2$ M.W.: 914.29, C(49.92%), H(3.96%), N(21.44%), S(7.01%), Zn(7.15%); found: C(49.85%), H(3.82%), N(21.25%), S(6.87%), Zn(7.03%); ^{1}H NMR (DMSO-d6) δ: 2.60(s, 3H, P_Z–C–CH_3), 3.09–3.36(s, 3H, P_Z–N–CH_3), 6.43(s, 2H, NH_2),10.82(s, 1H, OH), 7.35–7.68(m, 5H, Ph), 7.82–7.96(m, 3H, Ph), 8.61(s, 1H, N=CH); IR (KBr) ν (cm^{-1}): 3273(s) (NH_2), 706(m) (C–S), 1597(m) (C=N), 1602(w) (C–NO_2), 3464(s) (OH), 1262(m) (P_Z–C–CH_3), 1197(m) (P_Z–N–CH_3), 1453(m) (Ph–C=C), 1539(s) (Ph–C–C), 2951(s) (Ph–C–H), 462(s) (Zn–N), 345(m) (Zn-S).

3. Results and discussion

3.1. Physicochemical properties of the synthesized compounds

The ligands (**1a**–**1d**) were prepared by refluxing an appropriate amount of respective 4-(3′,4′-benzaldehydene)2-3-dimethyl-1-phenyl-3-pyrazolin-5-one with the corresponding semicarbazide/thiosemicarbazide in ethanol. The structures of the synthesized ligands were established with the help of their IR, NMR, and microanalytical data. All metal(II) complexes of Cu(II) and Zn(II) of these ligands were prepared by using the respective metal salts as chloride with the corresponding ligands in molar ratio of metal:ligand as 1:2 as obtainable in the following reaction.

$$M{\cdot}Cl_2{\cdot}nH_2O + 2L \rightarrow ML_2 + nH_2O + nHCl$$

where M = Cu(II) and Zn(II).

All these complexes are intensively coloured, air and moisture firm amorphous solids. They are insoluble in common organic solvents and only soluble in DMF and DMSO. Molar conductance values of the soluble complexes in DMF (10^{-3} M solution at 25 °C) indicate that the complexes have molar ratio of metal:ligand as 1:2. The lesser molar conductance values (0.93–4.32 $ohm^{-1}\,cm^{-2}\,mol^{-1}$) indicate that they are all non-electrolytic in nature. The elemental analyses data concur well with the planned formulae for the ligands and also recognized the [ML_2] composition of the metal(II) chelates.

3.2. Infrared spectral studies

In the current studies, semicarbazone/thiosemicarbazone related compounds are capable of exhibiting keto-enol tautomerism and react with metal cations to form metal complexes. The assignments of IR spectra of the ligands and their Cu(II) and Zn(II) complexes beside with their assignments are reported in Section 2. The broad band that appears in the range of 3069–3163 cm^{-1} is assigned to the stretching vibration of (N–H). A new prominent band at 1589–1626 cm^{-1}, due to azomethine ν(C=N) association appeared in all the ligands, indicates [15] that condensation between ketone moiety of 4-amino-2-3-dimethyl-1-phenyl-3-pyrazolin-5-one and that of amino group of semicarbazone/thiosemicarbazone has taken place ensuing into the creation of the desired ligands (**1a**)–(**1d**).

Moreover, on comparison of the IR spectra of the ligands with their Cu(II) and Zn(II) complexes showed [16] a major shift to lower wave numbers by 15–25 cm^{-1} in azomethine ν(C=N) suggesting involvement of the azomethine-N with Cu(II) and Zn(II) ion in the complexation. The band corresponding to the stretching vibration of the C=S group appears at 828–834 cm^{-1} in the ligand [17]. The absence of this band in the IR spectra of the metal complexes can be explained by the tautomerism of the C=S group with one of the imino groups to form the C–SH and the coordination of sulphur after deprotonation. The bands that appear in the range of 649–706 cm^{-1} and 1058–1098 cm^{-1} are thus assigned to the ν(C–S) and ν(C–O) respectively in the IR spectra of the metal complexes. These overall data suggest that the azomethine-N and enol/thiol-O or S groups are involved in coordination with the Cu(II) and Zn(II) ion complexes. In the low-frequency region, spectra of the Cu(II) and Zn(II) complexes exhibit [18] new bands which are not present in the spectra of the ligands. These bands are recognized to ν(M–O), ν(M–N) and ν(M–S).

Table 1
Electronic absorption spectral data of the ligands and their compounds.

Complex	Solvent	Absorption (cm^{-1})	Band assignment	Geometry
1a	EtOH	31,645	INCT[a]	–
		36,231	INCT	
		41,322	INCT	–
1b	EtOH	25,974	INCT	
		34,965	INCT	
		38,910	INCT	–
1c	EtOH	24,271	INCT	
		33,003	INCT	
		42,016	INCT	–
1d	EtOH	22,573	INCT	
		31,545	INCT	
		39,215	INCT	
[CuL_2**1a**]	DMF	11,148	$^2E_g \leftarrow {}^2T_{2g}$	Distorted octahedral
		26,178	INCT	
		40,161	INCT	
[CuL_2**1b**]	DMF	11,521	$^2E_g \leftarrow {}^2T_{2g}$	Distorted octahedral
		25,840	INCT	
		42,735	INCT	
[CuL_2**1c**]	DMF	15,385	$^2E_g \leftarrow {}^2T_{2g}$	Distorted octahedral
		27,397	INCT	
		39,683	INCT	
[CuL_2**1d**]	DMF	9709	$^2E_g \leftarrow {}^2T_{2g}$	Distorted octahedral
		28,249	INCT	
		38,168	INCT	

[a] INCT – intraligand charge transfer band.

3.3. ^{1}H NMR spectral studies

The ^{1}H NMR spectral data are reported along with the possible assignments in "experimental." All the protons were found as to be in their expected region [19]. The conclusions drawn from these studies lend further support to the mode of bonding discussed in their IR spectra. In the spectra of diamagnetic Zn(II) complexes, the resonance arising from the NH proton disappears, whereas that arising from the azomethine (HC=N) proton shifts to downfield values indicating the chelation of the ligands through the deprotonated enol/thiol-O/S groups and azomethine-N is established by downfield shifting of these signals in the Zn(II) complexes due to the increased conjugation and coordination [20].

3.4. Electronic spectral studies

The electronic spectra of the Cu(II) complexes (Table 1) showed one low-energy weak band around 9709–15,385 cm^{-1} and two strong high energy bands around 25,840–42,735 cm^{-1}. The low-energy band in this position typically expected for an octahedral configuration may be assigned to 10 Dq corresponding to the transition $^2E_g \leftarrow {}^2T_{2g}$ [21]. The strong high-energy band, in turn,

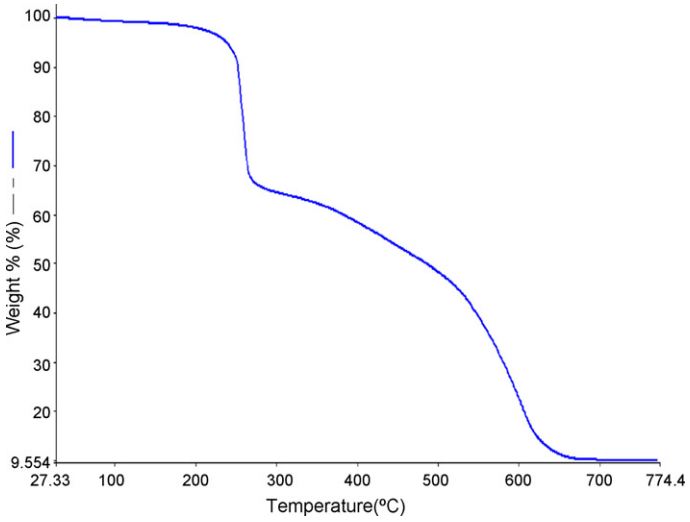

Fig. 1. The TGA curve of CuL_2[1d] complex.

is assigned to metal → ligand charge transfer. Also, the magnetic moment values (1.65–1.83 BM) for the CuL_2[1a–1d] complexes are indicative of antiferromagnetic spin–spin interaction through molecular association. Hence, the CuL_2[1a–1d] complexes appear to be in the distorted octahedral geometry with d_{x^2}–d_{y^2} ground state [22].

3.5. ESI-mass spectral studies

The electron impact mass spectrum of **1b** Schiff base shows a molecular ion peak *m*/*z* at 424 (M^+) with a relative intensity 15% which is equivalent to its molecular weight. The different pathways of the fragments of the parent molecular ion peaks are given in Scheme 3. The other molecular ion peaks appeared in the mass spectrum (abundance range from 1% to 100%) is attributed to the fragmentation of **1b** molecule obtained from the rupture of different bonds inside the molecule as shown in Scheme 3. The CuL_2[1b] complex gives a molecular ion peak at *m*/*z* 910(M^+) and *m*/*z* 911(M+1) with a relative intensity 10% and 7% respectively. The intensities of these peaks give the idea of the stability and abundance of the fragments. This type of stoichiometry (ML_2) is confirmed by the mass spectra of other complexes. This is in good agreement with the microanalytical data.

3.6. Thermal studies

Thermal stability and thermal behaviors of all complexes were studied by thermogravimetric analysis (TGA) at the atmosphere of nitrogen in the temperature range 25–900 °C. The correlations between the different decomposition steps of the complexes with the corresponding weight losses are discussed in terms of the proposed formula of the complexes [23–25]. The thermal behavior studies of all the complexes are almost same. Hence, the representative CuL_2[1d], ZnL_2[1d], CuL_2[1a] and ZnL_2[1a] complexes have been discussed. The representative thermogram of CuL_2[1d] is depicted in Fig. 1.

The TGA profiles over the temperature range 30–250 °C are usually due to loss of water of moisture, hydration and coordination. The complexes CuL_2[1d] and ZnL_2[1d] have first decomposition stage in the range 35–250 °C. This dehydration process probably is due to the loss of hydration water, which may be bound to hydroxyl group of the ligand by hydrogen bonds. Above 250 °C, CuL_2[1d] and ZnL_2[1d] decompose in a gradual manner, which may be due to fragmentation and thermal degradation of the organic moiety. The continuous loss of weights is observed up to 675 and 690 °C respectively. The final solid product of thermal decomposition is identified as respective metal oxide (found: 83.25%, calcd.: 83.39% for CuL_2[1d] and found: 84.52%, calcd.: 84.75% for ZnL_2[1d]). The CuL_2[1a] and ZnL_2[1a] complexes show no mass loss up to 182 °C, indicating the absence of water molecules and any other adsorptive solvents molecules in coordination sphere. The continuous loss of weight is observed up to 750 and 800 °C respectively; after that the weight of the product remains constant. The final weight losses in these cases agree with the formation of the respective metal oxides (found: 83.30%, calcd.: 83.52% for CuL_2[1a] and found: 84.57%, calcd.: 84.72% for ZnL_2[1a]).

From the above thermogravimetric analyses, the overall weight losses for the CuL_2[1d], ZnL_2[1d], CuL_2[1a] and ZnL_2[1a] complexes agree well with the proposed formula obtained by elemental analyses, IR, ^{1}H NMR, Mass and magnetic susceptibility measurements.

Table 2
The spin Hamiltonian parameters of Cu(II) complexes in DMSO at 300 and 77 K.

Complex	g-tensor			Hyperfine constant ($\times 10^{-4}$ cm^{-1})		
	$g_{\|\|}$	$g_\perp$	g_{iso}	$A_{\|\|}$	$A_\perp$	A_{iso}
$[CuL_2$[1b]]	2.6141	2.1289	2.2906	80	250	193
$[CuL_2$[1c]]	2.5969	2.1405	2.2926	90	260	203

3.7. EPR studies of Cu(II) complexes

To obtain further information about the stereochemistry and the site of the metal–ligand bonding and to determine the magnetic environment in the metal complexes, EPR studies of copper(II) complexes were carried out. Powder samples were used to record X-band EPR spectra of the Cu(II) complexes and the spectra were recorded in DMSO at liquid nitrogen temperature (LNT) and at room temperature (RT). The spin Hamiltonian parameters and bonding parameters of the Cu(II) complexes were calculated and are summarized in Tables 2 and 3.

In the present case, Cu(II) complexes, measured in polycrystalline sample at room temperature, give the following values: $g_{||} = 2.6141$, $g_\perp = 2.1289$ for the CuL_2[1b] and $g_{||} = 2.5969$, $g_\perp = 2.1405$ for CuL_2[1c]. The trend exhibits an auxiliary symmetric g-tensor parameters with $g_{||} > g_\perp > 2.0027$ indicating that the copper site has a $d_{x^2-y^2}$ ground state characteristic of octahedral geometry [26].

The parameter *G*, determined as $G = (g_{||} - 2)/(g_\perp - 2)$, which measures the exchange interaction between the metal centers in a polycrystalline solid, has been calculated. According to Hathaway et al. [27] if $G > 4$, the exchange interaction is negligible, but $G < 4$ indicates considerable exchange interaction in the solid complexes. The Cu(II) complexes reported in this paper give the "*G*" values which are greater than 4 indicating the exchange interaction is absent in solid complexes.

The observed values of α^2 and β^2 parameters indicate that the complexes have some covalent character and there is interaction in the out-of-plane π-bonding. The lower values of α^2 compared to β^2 indicate that the in-plane σ-bonding is more covalent than the in-plane π-bonding. For the present copper(II) complexes, the observed order $K_{||}$ is greater than $K_\perp$ implying a greater contribution from out-of-plane π-bonding than from in-plane π-bonding in metal–ligand π-bonding. Based on these observations, a distorted octahedral geometry is proposed for Cu(II) complexes. The

Table 3
The bonding parameters of Cu(II) complexes in DMSO solution.

Complex	α^2	β^2	γ^2	$K_{\|\|}$	$K_\perp$	*G*
$[CuL_2$[1b]]	0.9276	1.1463	0.9465	1.0632	0.8779	4.8446
$[CuL_2$[1c]]	0.9432	1.4632	1.3573	1.3800	1.2802	4.3120

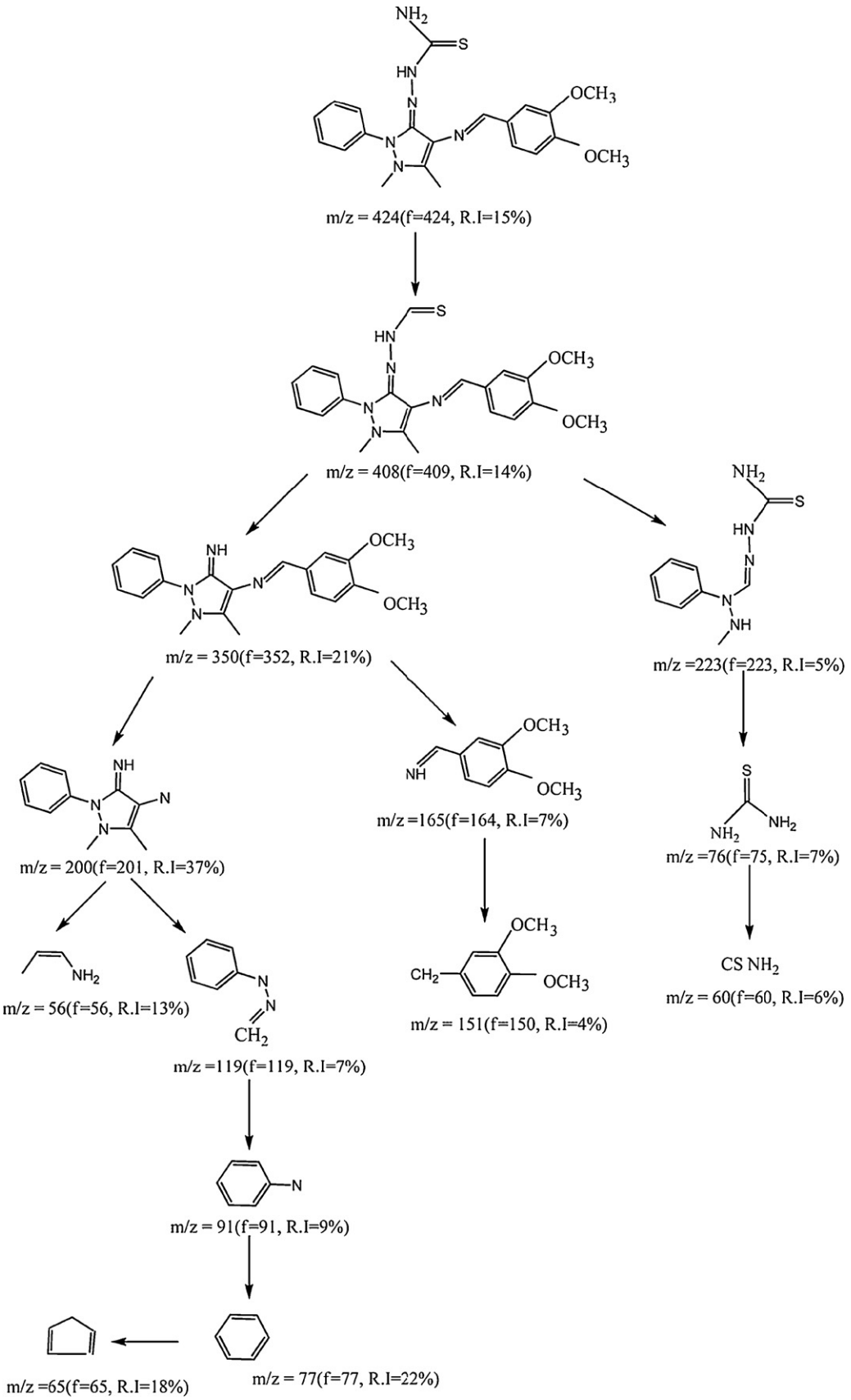

Scheme 3. Mass fragment pattern of **1b**.

EPR study of the Cu(II) complexes has provided supportive evidence to the conclusion obtained on the basis of electronic spectrum and magnetic moment value.

3.8. Biological activity

The antimicrobial activity results presented in Table 4 show that the newly synthesized compounds (**1a**–**1d**) and their Cu(II) and Zn(II) complexes possess biological activity. These new derivatives obtained by condensation of 4-(3′,4′-benzaldehydene)2-3-dimethyl-1-phenyl-3-pyrazolin-5-one with the corresponding semicarbazone/thiosemicarbazone (Scheme 2) were screened for their antibacterial activity against microorganisms. These results exhibited markedly an enhancement in activity on coordination with the metal ions against four testing bacterial strains. This enhancement in the activity is rationalized on the basis of the structures of (**1a**–**1d**) by possessing an additional azomethine (C=N) linkage which imports in elucidating the mechanism of transamination and resamination reactions in biological system [28]. It has also been suggested [29,30] that the ligands with nitrogen and oxygen donor systems might restrain enzyme production, since the enzymes which require these groups for their activity appear to be especially more susceptible to deactivation by the metal ions upon chelation. Chelation reduces the polarity [29,30] of the metal ion mainly because of the partial sharing of its positive charge with the donor groups and possibly the π-electron delocalization within the whole chelate ring system, thus formed during coordination. This process of chelation thus increases the lipophilic nature of the central metal atom, which in turn favors its permeation through the lipoid layer of the membrane. This in turn is responsible for increasing the hydrophobic character and liposolubility of the molecule in crossing cell membrane of the microorganism, and hence enhances the biological utilization ratio and activity of the testing drug/compound.

The order of inhibition with respect to metal ions of **1a**–**1d** is Cu > Zn. It is found that these complexes show strong antimicrobial activity at lower concentration when compared to earlier reported literature [31]. But some ZnL_2^{1b} and ZnL_2^{1c} have higher antibacterial activity for *B. subtilis* and *P. putita* respectively and ZnL_2^{1a} has higher antifungal activity for *R. stolonifer*, compared to the corresponding CuL_2^{1a} complex.

3.9. Oxidative cleavage of DNA

3.9.1. DNA cleavage activity comparison of the synthesized Cu(II) and Zn(II) complexes

In order to assess the competence of the Cu(II) and Zn(II) complexes for DNA strand scission, pBR322 DNA was incubated with individual Cu(II) and Zn(II) complexes under identical reaction conditions. The cleavage reaction was monitored by gel electrophoresis. The delivery of high concentrations of metal ion to the helix, in locally generating oxygen or hydroxide radicals, leads to an efficient DNA cleavage reaction. When circular pBR322 DNA is subjected to electrophoresis, DNA cleavage is monitored by relation of supercoiled circular pBR322 (form I) into nicked circular (form II) and linear (form III).

As shown in Fig. 2 all of the examined complexes are capable of promoting oxidative damage of DNA in the presence of H_2O_2 under physiological conditions (pH 7.2, 37 °C), but display different cleavage activities [32]. CuL_2^{1d} and CuL_2^{1c} reveal the highest DNA cleavage activity. Under the conditions we used, it can completely convert supercoiled form to nicked and linear form of DNA. CuL_2^{1b} also can switch supercoiled DNA to nicked and linear forms of DNA, but the supercoiled form is still seen. The difference in cleavage performance of the two complexes appears to be due to the attendance of nitro moiety in **1d** and **1c**. ZnL_2^{1d}, ZnL_2^{1b}, ZnL_2^{1c}, CuL_2^{1a} and ZnL_2^{1a} exhibit lesser activity than CuL_2^{1d}, CuL_2^{1c} and CuL_2^{1b}. These five complexes can only switch supercoiled form to nicked form. The difference in cleavage characteristics of these five complexes appears may be due to the attendance of methoxy moiety and nature of metal ions. The control experiments were carried out in the attendance of individual complexes together with DNA.

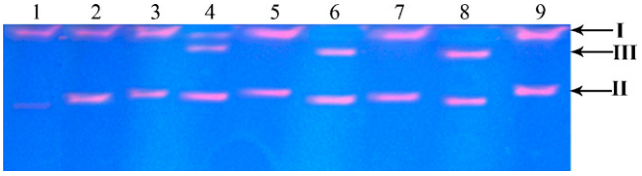

Fig. 2. Gel electrophoresis diagram showing the oxidative cleavage of SC pBR322 DNA (30 μM) by the Cu(II) and Zn(II) complexes of **1a**–**1d** in the presence of H_2O_2 in 50 mM Tris–HCl/NaCl buffer (pH 7.2) containing DMF. Lane 1, DNA control; lane 2, DNA + CuL_2^{1a} + H_2O_2; lane 3, DNA + ZnL_2^{1a} + H_2O_2; lane 4, DNA + CuL_2^{1b} + H_2O_2; lane 5, DNA + ZnL_2^{1b} + H_2O_2; lane 6, DNA + CuL_2^{1c} + H_2O_2; lane 7, DNA + ZnL_2^{1c} + H_2O_2; lane 8, DNA + CuL_2^{1d} + H_2O_2; lane 9, DNA + ZnL_2^{1d} + H_2O_2.

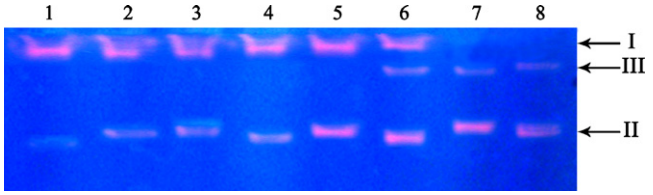

Fig. 3. Agarose gel electrophoresis pattern of supercoiled pBR322 DNA in the presence of concentration of CuL_2^{1d}, [H_2O_2] = 10 mM and light after irradiation at 365 nm for 30 min in 50 mM Tris–HCl/NaCl buffer (pH 7.2). Lane 1, DNA control; lane 2, DNA + CuL_2^{1d} (0.5 μM); lane 3, DNA + CuL_2^{1d} (1.0 μM); lane 4, DNA + CuL_2^{1d} (1.5 μM); lane 5, DNA + CuL_2^{1d} (2.0 μM); lane 6, DNA + CuL_2^{1d} (2.5 μM); lane 7, DNA + CuL_2^{1d} (3.0 μM); lane 8, DNA + CuL_2^{1d} (3.5 μM).

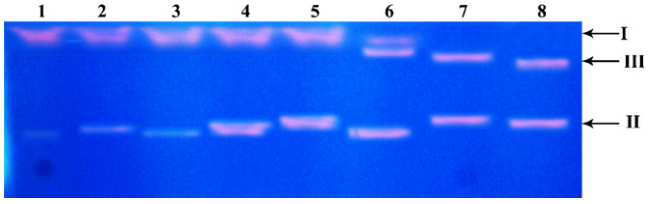

Fig. 4. Cleavage of supercoiled pBR322 DNA in the presence of CuL_2^{1d} (15 μM) complex and light after irradiation at 365 nm for 30 min in 50 mM Tris–HCl/NaCl buffer (pH 7.2). Lane 1, DNA control; lane 2, DNA + H_2O_2 (5 mM); lane 3, DNA + H_2O_2 (10 mM); lane 4, DNA + H_2O_2 (15 mM); lane 5, DNA + H_2O_2 (20 mM); lane 6, DNA + H_2O_2 (25 mM); lane 7, DNA + H_2O_2 (30 mM); lane 8, DNA + H_2O_2 (35 mM).

3.9.2. Effects of complex concentration on DNA cleavage

In order to investigate the influence of the concentration of CuL_2^{1d} or H_2O_2 on DNA cleavage reactions, two independent experiments were explored. In the first experiment, the concentration of H_2O_2 was kept constant and the concentration of the complexes was varied (Fig. 3); in the second experiment, the concentration of the complexes was kept constant and the concentration of H_2O_2 was varied (Fig. 4). All of the results indicate that the DNA cleavage activities of the complexes are obviously both complex and H_2O_2 concentration dependent. With the increase in complex or H_2O_2 concentration, the supercoiled DNA (SC DNA) decreases and is finally completely converted to nicked and linear forms. As also verified, the appearance of forms II and III depends on concentration of copper complex and H_2O_2.

3.9.3. Effect of irradiation time on DNA cleavage

Fig. 5 shows the gel electrophoresis separation of SC pBR322 DNA after incubation with the complexes CuL_2^{1d} and CuL_2^{1c} and

Table 4
The *in vitro* antimicrobial activity of ligand and their metal complexes (MIC in μg/mL).

Complex	Antibacterial activity[a]				Antifungal activity[a]			
	S. aureus	*B. subtilis*	*E. coli*	*P. putita*	*A. niger*	*R. stolonifer*	*C. albicans*	*R. bataicola*
1a	21.43	32.10	20.43	43.28	27.64	25.13	41.23	24.51
1b	21.34	34.51	28.36	22.41	36.19	37.24	27.38	45.23
1c	31.14	27.35	36.73	35.41	29.61	29.48	36.40	24.85
1d	28.65	36.12	23.76	29.54	31.02	41.21	27.54	26.81
[CuL_2 **1a**]	6.25	7.18	12.5	7.98	4.28	4.88	9.76	3.26
[ZnL_2 **1a**]	11.5	13.25	18.33	10.2	7.29	3.54	13.2	8.51
[CuL_2 **1b**]	7.28	6.74	5.42	8.67	4.28	12.4	5.37	11.40
[ZnL_2 **1b**]	17.23	5.98	13.0	11.8	8.52	9.48	8.12	10.51
[CuL_2 **1c**]	9.63	11.02	9.21	10.98	6.98	4.29	9.54	7.68
[ZnL_2 **1c**]	20.11	14.5	12.4	9.21	9.48	11.87	8.48	9.20
[CuL_2 **1d**]	10.94	9.76	7.67	11.5	5.67	7.63	4.89	7.84
[ZnL_2 **1d**]	17.0	10.15	11.54	12.14	9.58	16.52	9.94	12.01

[a] The MIC of standard drugs for antibacterial activity (Streptomycin) and antifungal activity (Nystatin) was found to be <2.45 μg/mL.

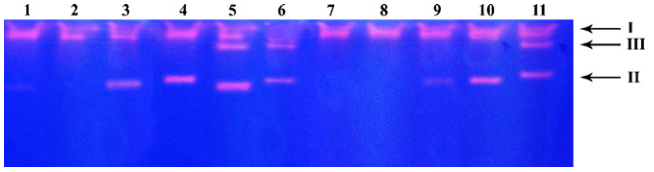

Fig. 5. Gel electrophoresis diagram showing the cleavage of SC pBR322 (0.5 μg) in the presence of CuL_2 **1d** and CuL_2 **1c** complexes (20 μM) in 50 mM Tris–HCl/NaCl buffer (pH 7.2) on photo-irradiation irradiation at 365 nm for 0, 20, 40, 60 and 80 min (lanes 2–6) for CuL_2 **1d** complex and (lanes 7–11) for CuL_2 **1c** complex, lane 1, DNA alone.

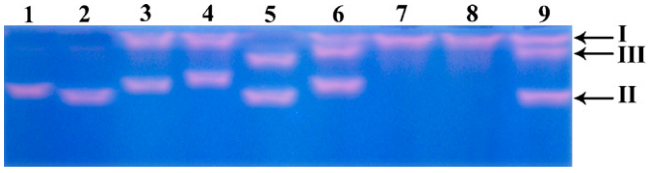

Fig. 6. Changes in the agarose gel electrophoretic pattern of pBR322 DNA (0.5 μg) in the presence of reducing agent 3-mercaptopropionic acid (MPA, 5 mM) in the dark in 50 mM Tris–HCl/NaCl buffer (pH 7.2) containing DMF. Lane 1, DNA control; lane 2, DNA + MPA; lane 3, DNA + CuL_2 **1d**; lane 4, DNA + CuL_2 **1c**; lane 5, DNA + CuL_2 **1d** + MPA; lane 6, DNA + CuL_2 **1c** + MPA; lane 7, DNA + CuL_2 **1d** + DMSO (2 μL) + MPA; lane 8, DNA + KI (5 μL) + CuL_2 **1c** + MPA; lane 9, DNA + NaN_3 (5 μL) + CuL_2 **1d** + MPA.

irradiation at 365 nm. At the same concentration of complex, with increasing irradiation time Form II and Form III also increase. Complete cleavage of DNA is observed with a 20 μM of complexes on 80 min exposure. It is known that ligands containing thio or thione moieties show efficient intersystem crossing to the triplet state on photo-irradiation and such an effect is found to be pronounced only when the sulphur is bonded to the metal center [33,34]. Similar results have been reported in other cases [35]. The different DNA cleavage efficiency of these two complexes may be due to the different binding affinity of the complexes to DNA [36].

3.9.4. *Effect of supercoiled pBR322 DNA by 3-mercaptopropionic acid (MPA)*

The DNA cleavage activity of the CuL_2 **1d** and CuL_2 **1c** complexes has been studied in the presence of MPA as reducing agent (Fig. 6). The CuL_2 **1d** and CuL_2 **1c** complexes efficiently cleave SC DNA in the presence of MPA, whereas, in the absence of MPA, do not show any significant cleavage of SC pBR322 DNA. Control experiments indicate the formation of the hydroxyl radical and/or copper-oxo species as the cleavage active species [37]. Control experiments using CuL_2 **1d** and CuL_2 **1c** have shown inhibition of cleavage in the presence of hydroxyl radical scavenger like DMSO or KI, while the singlet oxygen quencher, NaN_3, does not show any apparent effect

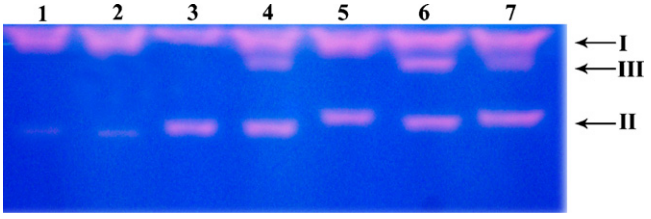

Fig. 7. Gel diagram showing the photocleavage of SC pBR322 DNA (0.5 μg) by using different reagents on monochromatic irradiations of wavelength at 365 nm for 30 min exposure with CuL_2 **1d** (25 μM) complex, [H_2O_2] = 10 mM in the presence of 50 mM Tris–HCl/NaCl buffer (pH 7.2). The reactions were carried out under aerobic conditions: lane 1, DNA control; lane 2, DNA + CuL_2 **1d**; lane 3, DNA + CuL_2 **1d** + H_2O_2; lane 4, DNA + NaN_3 (100 μM) + CuL_2 **1d**; lane 5, DNA + L-histidine (100 μM) + CuL_2 **1d**; lane 6, DNA + D_2O (14 μl) + CuL_2 **1d**; lane 7, DNA + DMSO (2 μl) + CuL_2 **1d**.

on the DNA cleavage activity indicating non-involvement of singlet oxygen species in the DNA cleavage reaction. The overall above observations may suggest that formation of hydroxyl radicals in the DNA cleavage reaction in the presence of MPA.

3.9.5. *Photoactivated cleavage of pBR322 DNA by CuL_2 **1d** complex*

There has been considerable interest in DNA endonucleolytic cleavage reactions that are activated by metal ions [38]. The photo-induced DNA cleavage activity of the complexes in the absence of MPA has been studied using UV light. Electrophoresis is carried out in a dark chamber for 15 min at 50 V in 50 mM Tris–HCl/NaCl buffer (pH 7.2). When circular plasmid DNA is subjected to electrophoresis, relatively fast migration will be observed for the supercoiled form (form I). If scission occurs on one strand (nicking), the supercoils will relax to generate a slower-moving open circular form (form II) [39]. If both strands are cleaved, a linear form (form III) will be generated that migrates between forms I and II [40]. Fig. 7 shows the gel electrophoretic separations of plasmid pBR322 DNA after incubation with CuL_2 **1d** complex and irradiation at 365 nm in the presence of varying radical scavengers (lanes 4–7). The CuL_2 **1d** complex is incubated with DNA, in the absence or in the presence of hydrogen peroxide as an oxidant agent. H_2O_2 itself can induce some single-strand scission in DNA molecules, as indicated by the small decrease in the concentration of supercoiled plasmid DNA (form I), and corresponding small increase in the concentration of relaxed circle (form II) as shown in Fig. 7 (lanes 2 and 3). To test the possibility that photo-induced cleavage involves the formation of singlet oxygen, which is known to react with guanine residues at neutral pH [41], the cleavage is tested in the presence of D_2O. Singlet oxygen would be expected to induce more strand scissions in D_2O than in H_2O due to its longer lifetime in the former solvent. It can also be seen in Fig. 7 that neither irradiation of DNA at 365 nm without CuL_2 **1d** nor incubation with CuL_2 **1d** without light

Table 5
Electrochemical behavior of copper(II) complexes in the presence of CT DNA.

Complex	Redox couple	I_{pc} (A) ($\times 10^{-5}$)		E_{pc} (V)		$E_{1/2}$ (V)		ΔE_p (V)		K_+/K_{2+}
		Free	Bound	Free	Bound	Free	Bound	Free	Bound	
[CuL_2**1a**]	Cu(III–II)	0.37	0.31	0.061	0.096	0.162	0.211	0.202	0.231	3.9
	Cu(II–I)	0.33	0.19	−0.454	−0.479	−0.276	−0.307	0.344	0.307	0.38
[CuL_2**1b**]	Cu(III–II)	2.28	1.73	0.197	0.265	0.531	0.519	0.668	0.509	14.1
[CuL_2**1c**]	Cu(II–I)	2.16	2.01	−0.965	−0.942	−0.791	−0.770	0.348	0.344	2.44
[CuL_2**1d**]	Cu(III–II)	0.23	–	0.166	–	0.241	–	0.150	–	–
	Cu(II–I)	0.37	0.32	−0.152	−0.175	–	–	–	–	0.41

yields significant strand scission. The DNA photocleavage studies of Cu(II) and Zn(II) complexes are consistent with earlier reports [42,43,10]

3.10. Magnetic measurement studies

The magnetic moments of the complexes were recorded at room temperature and the observed magnetic moment values for the Cu(II) complexes of **1a**–**1d** are 1.72, 1.83, 1.65 and 1.78 BM respectively. These values are agreeable to spin only value. Hence observed magnetic moment for the Cu(II) complexes under study indicates that they have distorted octahedral [44] configurations around metal ions. This is further supported by their electronic spectral data and CV studies.

3.11. DNA binding studies

DNA binding experiments were carried out in 0.5 mL Tris–HCl/NaCl buffer [50 mM Tris–HCl and 5 mM NaCl (pH 7.2)] using DMF solution (15 μL) of the complexes. Absorption titration measurements were done by varying the concentration of CT DNA but keeping the metal complex concentration as constant.

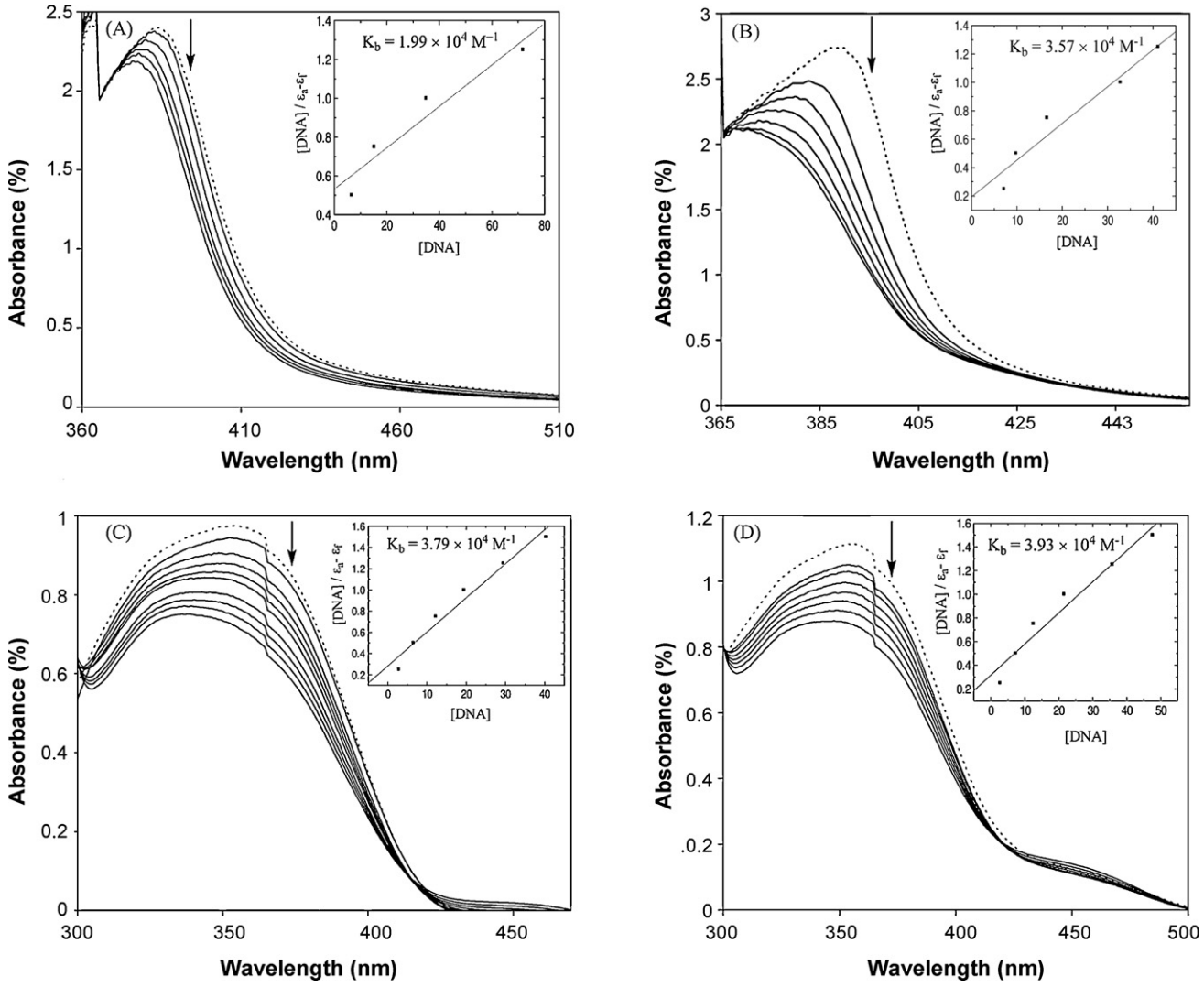

Fig. 8. Electronic spectra of Cu^{2+} complexes of (A) **1a**, (B) **1b**, (C) **1c** and (D) **1d** (10^{-3} M) in dimethylformamide in the absence (- - -) and presence (– – –)of CT DNA. Arrow shows that the absorbance changes upon increasing DNA concentrations. *Inset*: plots of [DNA]/($\varepsilon_a - \varepsilon_f$) *versus* [DNA] for the titration of CT DNA with the complexes.

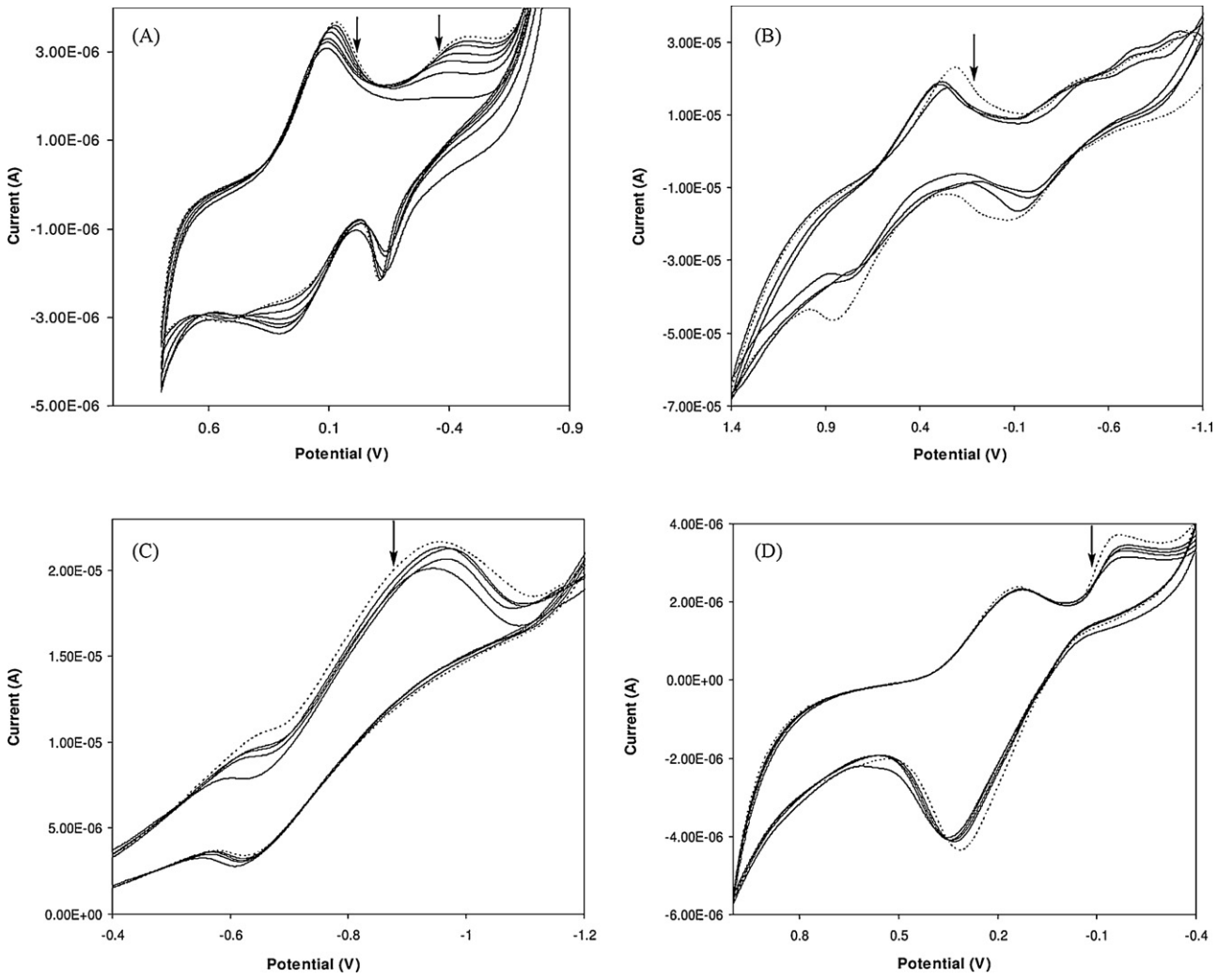

Fig. 9. Cyclic voltammogram at scan rate varying 0.05–0.250 V s^{-1} at 25 °C for Cu^{2+} complexes of (A) **1a**, (B) **1b**, (C) **1c** and (D) **1d** (10^{-3} M) in DMF containing 0.05 M *n*-Bu_4NClO_4 as supporting electrolyte at a Pt disc working electrode.

The different modes of interaction of a metal complex with DNA can be studied not only by this technique but also by cyclic voltammetry (CV) and differential pulse voltammetry (DPV). These were employed to probe the binding of metal complexes to DNA in solution. DPV data were used to obtain quantitative information about the interaction of these metal complexes with CT DNA.

Viscosity experiments were carried out using an Ubbelodhe viscometer maintained at a constant temperature at 30.0 ± 0.1 °C in a thermostatic water bath. Flow time was measured with a digital stopwatch, and each sample was measured three times, and an average flow time was calculated. Data were presented as $(\eta/\eta^0)^{1/3}$ *versus* binding ratio [45], where η is the viscosity of CT DNA in the presence of complex, and η^0 is the viscosity of CT DNA alone.

3.11.1. Absorption spectra studies

The application of electronic absorption spectroscopy in DNA binding studies is one of the most useful techniques [46] is carried out at 25 ± 2 °C. The electronic spectral trace of Cu(II) complexes titrated with DNA are given in Fig. 8. Complex binding with DNA through intercalation usually results in hypochromism and blue shift, due to the intercalative mode involving a strong stacking interaction between an aromatic chromophore and the base pairs of DNA. The extent of the hypochromism commonly parallels the intercalative binding strength. In order to compare quantitatively the binding strength of the copper complexes, the intrinsic binding constants K_b of the copper complexes with DNA were obtained by monitoring the changes in absorbance with increasing concentra-

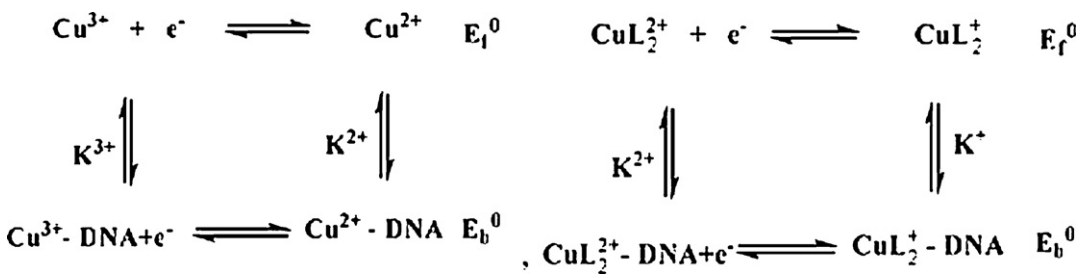

Scheme 4. A Nernstian electron transfer to a system in which both the oxidized and reduced forms are associated with a third species in solution (DNA).

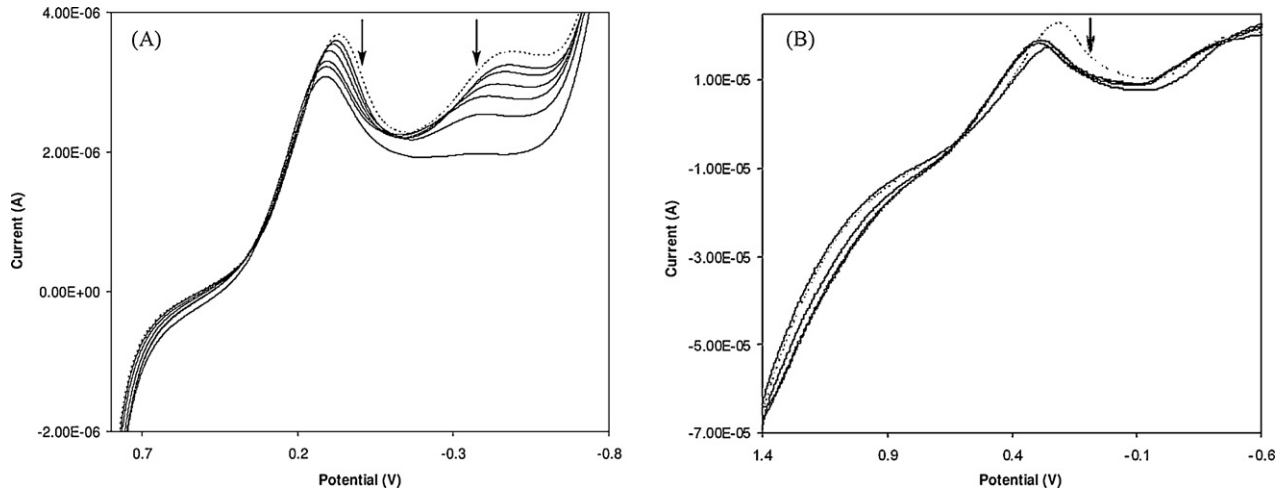

Fig. 10. Differential pulse voltammograms of (10^{-3} M) mol L^{-1} of Cu^{2+} complexes of (A) **1a** (scan rate 0.05 V s^{-1}) and (B) **1b** (scan rate 0.250 V s^{-1}) with incremental addition of DNA in DMF–Tris–HCl/NaCl buffer solution (pH 7.2).

tion of DNA using the following equation:

$$\frac{[DNA]}{\varepsilon_a - \varepsilon_f} = \frac{[DNA]}{\varepsilon_b - \varepsilon_f} + \frac{1}{K_b(\varepsilon_b - \varepsilon_f)}$$

where [DNA] is the concentration of DNA in base pairs, the apparent absorption coefficients ε_a, ε_f and ε_b correspond to A_{obs}/[Cu], the extinction coefficient for the free copper complexes and the extinction coefficient for the free copper complexes in the fully bound form respectively. In plots of [DNA]/($\varepsilon_a - \varepsilon_f$) *versus* [DNA], K_b is given by the ratio of slope to the intercept [47–49]. Intrinsic binding constants K_b of copper complexes of **1a**–**1d** are obtained as 1.99×10^4, 3.57×10^4, 3.79×10^4 and 3.93×10^4 M^{-1} respectively. Our results are consistent with earlier reports on preferential binding to CT DNA in the copper complexes [50–53].

3.11.2. Electrochemical studies

Table 5 summarizes the electrode potentials for all complexes of Cu(II) in DMF. The cyclic voltammetric studies provide an insight to the CT DNA binding. Typical CV behavior of series of Cu(II) complexes of **1a**–**1d** in the absence and presence of CT DNA is shown in Fig. 9. The difference between forward and backward peak potentials can provide a rough evaluation of the degree of the reversibility of one electron transfer reaction. The analysis of cyclic voltammetric responses with the scan rate varying 50–250 mV/s gives the evidence for a quasi-reversible one electron oxidation. The decreased extents of the peak currents observed for all Cu(II) complexes upon addition of CT DNA indicate that complexes interact with DNA through intercalating way. The Nernst equation can be used to estimate the ratio of equilibrium constants for the binding of the oxidative and reductive ions to DNA according to the literature [54]

$$E^{\circ}_b - E^{\circ}_f = 0.0591 \log\left(\frac{K_{red}}{K_{ox}}\right)$$

The drop of the voltammetry currents in the presence of DNA may be attributed to slow diffusion of the metal complex bound to CT DNA. This in turn indicates the extent of binding affinity of the complex to DNA.

In the cyclic voltammogram of CuL_2 **1a**, in the absence of DNA two well-defined quasi-reversible one electron cyclic responses have been observed at E_{pc} = 0.061 V with a corresponding oxidation peak at E_{pa} = 0.263 V [Cu(III)/Cu(II)] and at E_{pc} = −0.454 V with a corresponding oxidation peak at E_{pa} = −0.098 V [Cu(II)/Cu(I)] respectively. The ratio of cathodic to anodic peak height is less than one. When CT DNA is added to a solution of Cu(II) complex of **1a**, marked decreases in the peak current heights and shifts of peak potentials to more negative values are observed [55]. The shift in reduction peak potential observed between the reduction of Cu(III)/Cu(II) and reduction of Cu(II)/Cu(I) in complex of **1a** (Scheme 4) is indicative for strong copper binding.

The cyclic voltammogram recorded for the CuL_2 **1b**, reveals one electron quasi-reversible Cu(III)/Cu(II) wave with $E_{1/2}$ values as 0.531 and 0.519 V for free and bound forms respectively. In the absence of DNA, the complex involves single redox step corresponding to Cu(III)/Cu(II) at E_{pc} = 0.197 V and the associated anodic peak at E_{pa} = 0.865 V. On addition of CT DNA, the complex experiences a shift in $E_{1/2}$ as well as in E_p values. The ratio of I_{pa}/I_{pc} for the bound complex of **1b** is less than unity, suggesting that CT DNA is bound strongly to the complex. In addition to the changes in the formal potential, the voltammetric peak decreases upon addition of CT DNA to the complex. The decrease in the current is due to the diffusion of the equilibrium mixture of free and DNA-bound metal complex to the electrode surface [56]. In the absence of DNA one extra anodic peak is appeared at −0.077 V and no reduction peak, suggesting that unstabilization of Cu(I) species may be due to no d–π interactions between the copper-d orbitals and the aromatic π-system rather than Cu(II) species.

In the absence of DNA, the electrochemical behavior of CuL_2 **1c** shows a redox process corresponding to the Cu(II)/Cu(I) couple at E_{pa} = −0.617 V and the associated cathodic peak at E_{pc} = −0.965 V. The addition of CT DNA causes diminution of the peak currents of the reduction of Cu(II)/Cu(I). It is due to variation of the binding state and the slower mass transfer of complex bound to DNA fragments. It has been shown that binding of the metal complex to DNA can bring about a shift in the redox potential due to its intercalative binding with DNA which indicates that the reaction of the complex with DNA on the GC electrode is a diffusion controlled quasi-reversible redox process.

The CuL_2 **1d** exhibits one quasi-reversible peak in the absence of DNA. The representative cyclic voltammogram of Cu(II) complex displays two reduction peaks, one at E_{pc} = 0.166 V with an associated oxidation peak at E_{pa} = 0.316 V, second reduction peak at E_{pc} = −0.152 V with no associated oxidation peak corresponding to the Cu(III)/Cu(II) and Cu(II)/Cu(I) respectively. The incremental addition of CT DNA to the complex the second cathodic peak causes a shift in the potential and decrease in the current intensity, but in the first cathodic peak there is no significant change in the potential as well as current intensity, suggesting that the changes of peak currents of the reduction of Cu(II)/Cu(I) observed for CuL_2 **1d** may

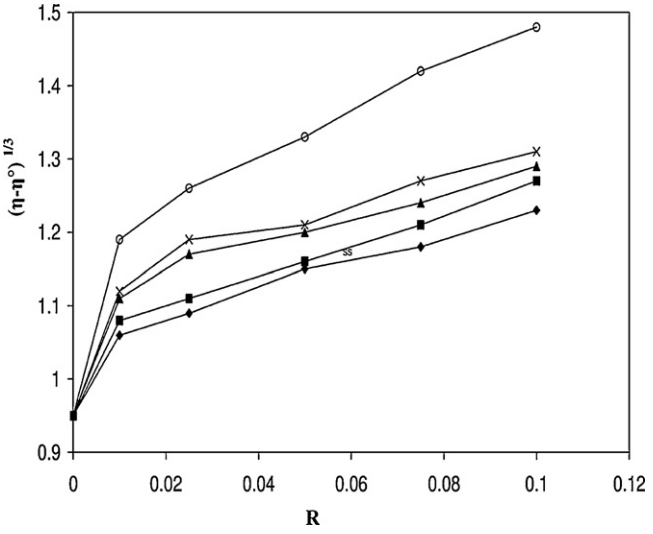

Fig. 11. Effect of increasing amounts of EB (○) and in the presence of increasing concentrations of copper complexes of CuL_2**1d** (♦), CuL_2**1c** (■), CuL_2**1b** (▲) and CuL_2**1a** (×) on the relative viscosity of CT DNA at 30 °C. [DNA] = 1.5 mM, R = [complex]/[DNA] or [EB]/[DNA].

indicate that complex possesses higher DNA binding affinity with complex.

3.11.3. Differential pulse voltammetry (DPV)

Differential pulse voltammogram (DPV) of the CuL_2**1a** and CuL_2**1b** both in the presence and in the absence of DNA is given in Fig. 10. The peak potential and current of the both complexes are changed in the presence of DNA. K_+/K_{2+} value for the copper complexes suggesting that the preferential stabilization of Cu(II) form over Cu(III) and Cu(I) form on binding to DNA. DPV of the complexes as a function of added DNA also indicates a large decrease in current intensity with a small shift in formal potential due to the intercalative interaction of complexes.

3.11.4. Viscosity measurements

The bonding between the complexes and DNA is further elucidated by viscosity measurements. Optical photophysical probes generally provide necessary, but insufficient clues to support a

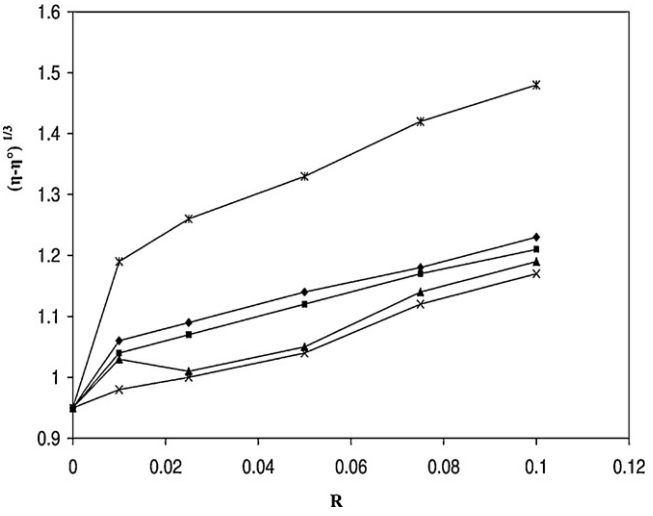

Fig. 12. Effect of increasing amounts of EB (*) and in the presence of increasing concentrations of zinc complexes of ZnL_2**1d** (×), ZnL_2**1c** (▲), ZnL_2**1b** (■) and ZnL_2**1a** (♦) on the relative viscosity of CT DNA at 30 °C. [DNA] = 1.5 mM, R = [complex]/[DNA] or [EB]/[DNA].

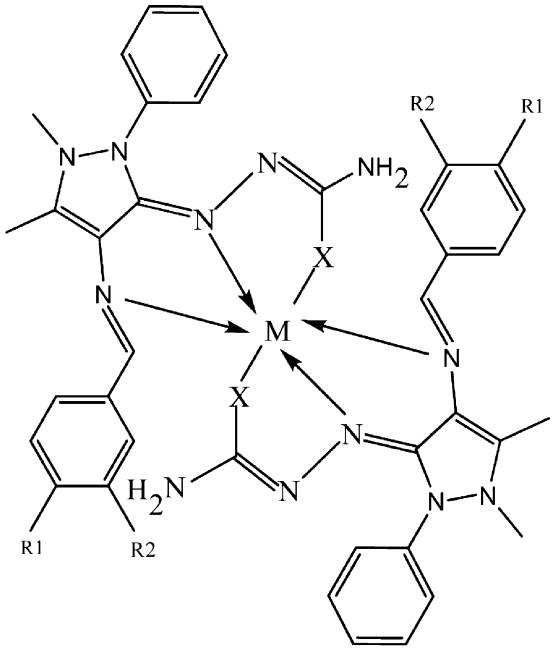

Fig. 13. Molecular structure of the complex, where M = Cu^{2+} and Zn^{2+}.

binding model of Cu(II) and Zn(II) complexes with DNA. A classical intercalation mode causes a significant increase in viscosity of DNA due to an increase in separation of base pairs at intercalation sites and hence an increase in overall DNA length [57]. The well-known DNA intercalator ethidium bromide (EB) increases the viscosity of DNA with increments of the concentration. On the other hand, the viscosity of DNA increases dramatically upon addition of the title complexes. The changes in relative viscosity of CT DNA in the presence of complexes Cu(II), Zn(II) and EB are shown in Figs. 11 and 12. The increased degree of viscosity, which may depend on its affinity to DNA follows the order of EB > **1a** > **1b** > **1c** > **1d**, which is consistent with the above results of Cu(II) and Zn(II) proposes to be bound to DNA by intercalation [42,10].

4. Conclusions

Based on the above observations of the elemental analysis, molar conductivity, UV–vis, magnetic, IR and ^{1}H NMR spectral data it is possible to determine the type of coordination of the ligands in their metal complexes. The spectral data show that all the Schiff bases exist as tridentate ligands by bonding to the metal ion through the deprotonated enol/thiol-O/S groups and azomethine nitrogen. The analytical data show the presence of one metal ion per two ligand molecules and suggest a mononuclear structure for the complexes. The correlation of the experimental data allows assigning an octahedral stereochemistry to all the above synthesized complexes as shown in Fig. 13. Cu(II) and Zn(II) complexes have been synthesized and their abilities to induce oxidatively generated DNA damage are compared. The observed efficient photonuclease activity of CuL_2**1d** under UV light on short exposure time and with a lesser concentration of the metal complex is a significant result in the chemistry of copper-based nucleolytic agents. Electronic spectra, cyclic voltammetry, differential pulse voltammogram and viscosity measurements indicate that the complexes bind to DNA by intercalative modes. It is found that the metal complexes have more biological activity than the free ligands.

Acknowledgments

The authors express their sincere thanks to the College Managing Board, Principal and Head of the Department of Chemistry, VHNSN College, for providing necessary research facilities and financial support.

References

[1] M.M.B. Pessoa, G.F.S. Andrade, V.R.P. Monteiro, M.L.A. Temperini, Polyhedron 20 (2001) 3133–3141.
[2] A.E. Liberta, D.X. West, Biometals 5 (1992) 121–126.
[3] N. Raman, R. Jeyamurugan, B. Raj kapoor, V. Mehesh, Appl. Organometal. Chem. 23 (2009) 283–290.
[4] M.A. Jakupec, M. Galanski, B.K. Keppler, Rev. Physiol. Biochem. Pharmacol. 146 (2003) 1–53.
[5] L. Giovagnini, L. Ronconi, D. Aldinucci, D. Lorenzon, S. Sitran, D. Fregona, J. Med. Chem. 48 (2005) 1588–1595.
[6] J.R. Dimmock, S.C. Vashishtha, J.P. Stables, J. Med. Chem. 35 (2000) 241–248.
[7] T. Klimova, E.I. Klimova, M. Mertinez Garcia, J.M. Mendez stivalet, L.R. Ramirez, J. Organomet. Chem. 633 (2001) 137–142.
[8] N. Bharti, K. Husain, M.T. Gonzalez Garza, D.E. Cyuz-Vega, J. Castro-Garza, Bioorg. Med. Chem. Lett. 12 (2002) 3475–3478.
[9] B. Peter, B. Roman, M. Breza, H. Elias, H. Fuess, V. Jorik, R. Klement, I. Svoboda, Polyhedron 21 (2002) 1561–1571.
[10] A.K. Patra, S. Roy, A.R. Chakravarty, Inorg. Chim. Acta 362 (2009) 1591–1599.
[11] Vogel A Text Book of Quantitative Inorganic Analysis, third ed., ELBS, Longman, London, 1969.
[12] L.G. Van Waasbergen, I. Fajdetic, M. Fianchini, H.V. Rasika dias, J. Inorg. Biochem. 101 (2007) 1180–1183.
[13] D. Liu, K. Kwasniewska, Bull. Environ. Contam. Toxicol. 27 (1981) 289–294.
[14] R.N. Patel, N. Singh, K.K. Shukla, U.K. Chauhan, S. Chakraborty, J. Niclos-Gutierrez, A. Castineiras, J. Inorg. Biochem. 98 (2004) 231–237.
[15] L.J. Bellamy, The Infrared Spectra of Complex Molecules, John Wiley & Sons, New York, NY, 1971.
[16] J.R. Ferrero, Low-Frequency Vibrations of Inorganic and Coordination Compound, John Wiley & Sons, New York, NY, 1971.
[17] P. Bindu, M.R. Kurup, T.R. Satyakeerty, Polyhedron 18 (1998) 321–331.
[18] K. Nakamoto, Infrared Spectra of Inorganic and Coordination Compounds, second ed., Wiley Interscience, New York, NY, 1970.
[19] W.W. Simmons, The Sadtler Handbook of Proton NMR Spectra, Sadtler Research Laboratories, Philadelphia, PA, 1978.
[20] D.J. Pasto, Organic Structure Determination, Prentice Hall, London, UK, 1969.
[21] V. Reddy, N. Patil, T. Reddy, S.D. Angadi, Eur. J. Chem. 5 (2008) 529–538.
[22] C.J. Ballhausen, An Introduction to Ligand Field Theory, McGraw Hill, New York, NY, 1962.
[23] F. Karipcin, E. Kabalcılar, Acta Chim. Slov. 54 (2007) 242–247.
[24] M.M. Omar, G.G. Mohamed, Spectrochim. Acta Part A 61 (2005) 929–936.
[25] M. Thankamony, B. Sindhu Kumari, G. Rijulal, K. Mohanan, J. Therm. Anal. Calorim. 95 (2009) 259–266.
[26] G. Speir, J. Csihony, A.M. Whalen, C.G. Pierpont, Inorg. Chem. 35 (1996) 3519–3524.
[27] B.J. Hathaway, J.N. Bardley, R.D. Gillard (Eds.), Essays in Chemistry, Academic Press, New York, NY, USA, 1971.
[28] P.P. Dholakiya, M.N. Patel, Synth. React. Inorg. Met.-Org. Chem. 34 (2004) 553–563.
[29] Z.H. Chohan, Appl. Organometal. Chem. 20 (2006) 112–116.
[30] Z.H. Chohan, M. Arif, Z. Shafiq, M. Yaqub, C.T. Supuran, J. Enzyme Inhib. Med. Chem. 21 (2006) 95–103.
[31] P.V. Rao, A.V. Narasaiah, Indian J. Chem. A 42 (2003) 1896–1899.
[32] V.G. Vaidyanathan, B. Unni Nair, J. Inorg. Biochem. 93 (2003) 271–276.
[33] X. Qian, T.B. Huang, D.-Z. Wei, D.-H. Zhu, M.-C. Fan, W. Yao, J. Chem. Soc., Perkin Trans. 2 (2000) 715–718.
[34] A. Jacobs, J. Piette, J. Photochem. Photobiol. B 22 (1994) 9–15.
[35] K. Li, L.H. Zhou, J. Zhang, S.Y. Chen, Z.W. Zhang, J.J. Zhang, H.H. Lin, X.Q. Yu, Eur. J. Med. Chem. 44 (2009) 1768–1772.
[36] X.L. Wang, H. Chao, H. Li, X.L. Hong, Y.-J. Liu, L.N. Ji, Trans. Met. Chem. 30 (2005) 305–311.
[37] T.B. Thederahn, M.D. Kuwabara, T.A. Larsen, D.S. Sigman, J. Am. Chem. Soc. 111 (1989) 4941–4946.
[38] R.P. Hertzberg, P.B. Dervan, J. Am. Chem. Soc. 104 (1982) 313–315.
[39] J.K. Barton, A.L. Raphael, J. Am. Chem. Soc. 106 (1984) 2466–2468.
[40] X. QianHe, Q. YueLin, R. DingHu, X. HongLu, Spectrochim. Acta Part A 68 (2007) 184–190.
[41] P.A.N. Reddy, B.K. Santra, M. Nethaji, A.R. Chakravarty, J. Inorg. Biochem. 98 (2004) 377–386.
[42] P. Xi, Z. Xu, F. Chen, Z. Zeng, X. Zhang, J. Inorg. Biochem. 103 (2009) 210–218.
[43] A. Hangan, A. Bodoki, L. Oprean, G. Alzuet, M. Liu-González, J. Borrás, Polyhedron 29 (2010) 1305–1313.
[44] N.S. Biradar, B.R. Havinale, Inorg. Chim. Acta 17 (1979) 157–160.
[45] G. Cohen, H. Eisenberg, Biopolymers 8 (1969) 45–49.
[46] J.K. Barton, J.J. Dannenberg, A.L. Raphael, J. Am. Chem. Soc. 106 (1984) 2172–2176.
[47] L.F. Tan, H. Chao, Y.F. Zhou, L.N. Ji, Polyhedron 26 (2007) 3029–3036.
[48] L.F. Tan, X.H. Liu, H. Chao, L.N. Ji, J. Inorg. Biochem. 101 (2007) 56–63.
[49] Y.J. Liu, H. Chao, Y.X. Yuan, H.J. Yu, L.N. Ji, Inorg. Chim. Acta 359 (2006) 3807–3814.
[50] Y.H. Li, B.D. Wang, Z.Y. Yang, Spectrochim. Acta Part A 67 (2007) 395–401.
[51] A.K. Patra, M. Nethaji, A.R. Chakravarty, J. Inorg. Biochem. 101 (2007) 233–244.
[52] F. Arjmand, M. Aziz, Eur. J. Med. Chem. 44 (2009) 834–844.
[53] N. Raman, R. Jeyamurugan, A. Sakthivel, L. Mitu, Spectrochim. Acta Part A 75 (2010) 88–97.
[54] M.T. Carter, M. Rodriguez, A.J. Bard, J. Am. Chem. Soc. 111 (1989) 8901–8911.
[55] R. Jain, S. Gupta, Bull. Electrochem. 14 (1998) 57–61.
[56] T.W. Weltch, H.H. Tholp, J. Phys. Chem. 100 (1996) 13829–13836.
[57] B. Peng, X. Chen, K.J. Du, B. LeYu, H. Chao, L. NianJi, Spectrochim. Acta Part A 74 (2009) 896–901.